# Evolution of Shape Complementarity and Catalytic Efficiency from a Primordial Antibody Template

Jian Xu,[1]* Qiaolin Deng,[2] Jiangang Chen,[2] Kendall N. Houk,[2] Johannes Bartek,[3] Donald Hilvert,[3] Ian A. Wilson[1]

**The crystal structure of an efficient Diels-Alder antibody catalyst at 1.9 angstrom resolution reveals almost perfect shape complementarity with its transition state analog. Comparison with highly related progesterone and Diels-Alderase antibodies that arose from the same primordial germ line template shows the relatively subtle mutational steps that were able to evolve both structural complementarity and catalytic efficiency.**

Complementarity between enzyme and transition state is the essence of biological catalysis (*1*). The development of catalytic antibodies, in which the microevolutionary processes of the immune system are exploited to generate immunoglobulins complementary to transition-state analogs (*2*), is a practical embodiment of this insight. This approach has been particularly useful as a source of catalysts for transformations, such as Diels-Alder cycloadditions (*3*), that are rare or unknown in nature. Because of the large body of genetic and structural information for antibodies, these systems also provide an opportunity for analyzing the evolution and mechanism of catalysis by proteins (*4*). Here, we present a detailed structural, mechanistic, and quantum mechanical computational study of 1E9, the most active Diels-Alderase antibody known (*5*) to establish the origin of its catalytic efficiency.

Antibody 1E9 was generated (*5*) against the endo hexachloronorbornene derivative **6**, a stable analog of transition state **5** for the [4+2] cycloaddition between tetrachlorothiophene dioxide (TCTD; **1**) and *N*-ethylmaleimide (NEM; **2**) (Fig. 1A). The 1E9 reaction proceeds in two steps (*6*); the initial high-energy intermediate **3** spontaneously eliminates sulfur dioxide to give a product that readily undergoes air oxidation to form *N*-ethyltetrachlorophthalimide **4**. Because planar **4** is structurally so different from transition state **5**, product inhibition is effectively minimized. As judged by originally reported $k_{cat}/k_{uncat}$ values in excess of 100 M (*5*), 1E9 is significantly more efficient than other reported Diels-Alderase antibodies (*7–10*) as well as ribozymes selected for their ability to promote cycloadditions (*11*).

The Fab fragment of 1E9 was prepared by proteolytic digestion of the murine immunoglobulin G1 (IgG1) (*12*), and the crystal structure of its complex with **6** was determined to 1.9 Å (Table 1). The rigid hexachloronorbornene portion of the hapten was clearly evident in the initial $F_o - F_c$ omit map (Fig. 2). The hapten binds edge on in a hydrophobic pocket of complementary shape (Fig. 3A). Excluding the linker, 86.3% of its surface is buried upon binding, and the fit between protein and ligand is so snug that no interfacial cavities are discernable, even with a 1.2 Å radius probe. Ligand recognition is achieved through 121 van der Waals contacts of the hexachloronorbornene moiety with the peptide backbone and the side chains of multiple aliphatic and aromatic residues (Figs. 3A and 4). Notable in this regard is the π-stacking interaction between the succinimide group of the hapten, which corresponds to the maleimide substrate, and the indole ring of $Trp^{H50}$. The only polar residues in the binding pocket are the highly conserved $Asn^{H35}$ of the VGAM3.8 family, which donates a hydrogen bond to the more deeply buried of the succinimide carbonyl groups of **6**, and $Ser^{L91}$, which is directed away from the ligand.

Sequencing and cross-reactivity studies (*13*) previously revealed 1E9 to be closely

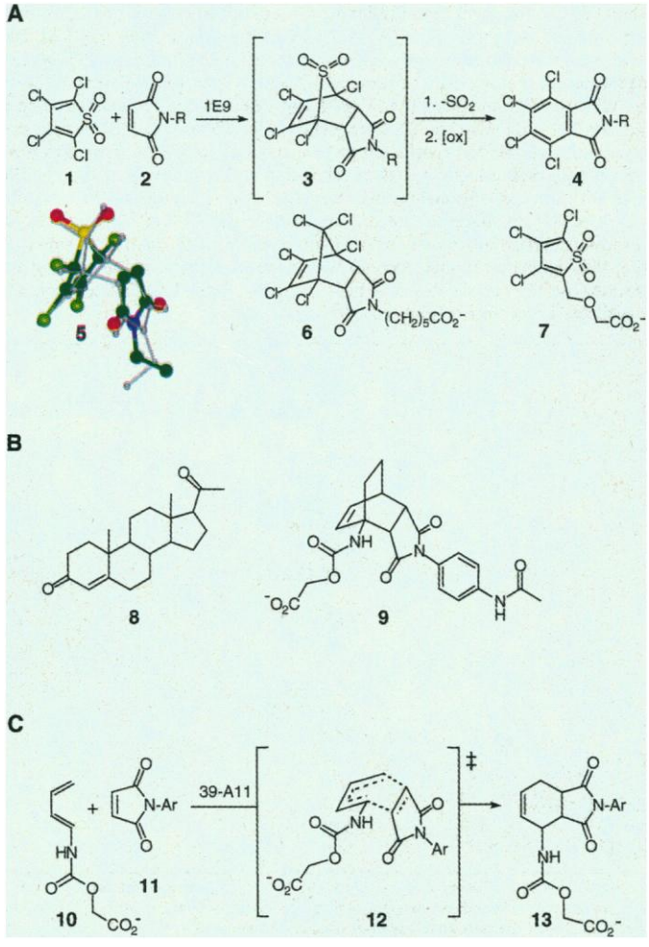


**Fig. 1.** Comparison of the Diels-Alder reactions catalyzed by antibodies 1E9 and 39-A11. **(A)** In 1E9, TCTD **1** reacts with NEM **2**, via transition state **5** (in color overlaid with hapten **6** in gray), to form intermediate **3**. Elimination of sulfur dioxide, which occurs through a similarly structured, second transition state, and oxidation give **4** as the final product. The transition state analog **6** is the hapten used to raise antibody 1E9. Water-soluble compound **7** is an alternative diene substrate for 1E9, designed by consideration of the crystal structure. **(B)** Steroid hapten **8** of another related antibody, DB3, and transition state anolog **9** used to generate 39-A11. **(C)** Diels-Alderase antibody 39-A11 catalyzes the reaction between **10** and **11**, through transition state **12**, to give cyclohexene **13** as the final product.

[1]Department of Molecular Biology and Skaggs Institute for Chemical Biology, The Scripps Research Institute, 10550 North Torrey Pines Road, La Jolla, CA 92037, USA. [2]Department of Chemistry and Biochemistry, University of California, Los Angeles, 405 Hilgard Avenue, Los Angeles, CA 90095–1569, USA. [3]Laboratory of Organic Chemistry, Swiss Federal Institute of Technology (ETH), Universitätstrasse 16, CH-8092 Zurich, Switzerland.

*Present address: Molecular Simulations Inc., 9685 Scranton Road, San Diego, CA 92121, USA.

related to DB3, an antibody to progesterone (*14*). This similarity apparently extends to several other antibodies derived from the same polyspecific germ line sequences, most notably Diels-Alder catalyst 39-A11, which was raised against a bicyclo[2.2.2]octene transition state analog **9** (Fig. 1, B and C) (*15*). What is striking about the 1E9·**6** complex, compared with the DB3·**8** (*15*) and 39-A11·**9** (*15*) structures, is the almost perfect shape complementarity between protein and ligand (Fig. 3). We have quantified shape complementarity by defining a gap index (angstroms) that represents the gap volume between hapten and antibody (cubic angstroms) divided by buried surface (square angstroms). The 1E9·**6** gap index of 0.44 Å is substantially less than those of either DB3 or 39-A11 (Table 2) or other representative biological complexes, such as enzyme-inhibitor (2.20 ± 0.47 Å) and antibody-protein complexes (3.02 ± 0.8 Å) (*16*), further underscoring the remarkably tight hand-in-glove-like fit for 1E9 and its hapten. Molecular docking experiments (*17*) with 1E9 and DB3 suggest that noncognate ligands bind randomly in the apolar cavity, whereas the cognate hapten is oriented through a hydrogen bond to $Asn^{H35}$ and adopts a single, well-defined binding mode similar to that in the crystal structure. Specificity in these systems appears to be conferred by a small number of mutations in the shared scaffold.

The heavy and light chains of 1E9, DB3, and 39-A11 are derived from the highly restricted *VGAM3.8* and $V_K$5.1 gene families (*13–15*). The mature 1E9 sequence differs from the putative germ line genes (*VFM11* and $V_K$5.1) by eight somatic mutations in the heavy chain and six in the light chain (*13*). Of the altered residues, only two ($Ser^{L89}$ → Phe and $Trp^{H47}$ → Leu) make direct contact with the hapten and are unique to 1E9 (Fig. 4). The $Ser^{L89}$ → Phe somatic mutation significantly improves shape complementarity between 1E9 and **6** and eliminates a prominent cavity present in the 39-A11 and DB3 complexes (Fig. 3). This mutation also increases the hydrophobicity of the combining site, favoring binding of the apolar ligand. The substitution of framework residue $Trp^{H47}$ by Leu is a particularly rare mutation; of 150 antibodies in the database, 138 have a Trp at position H47 (*18*). This change dramatically alters the shape of the binding pocket of 1E9 compared with DB3 and 39-A11 (Fig. 3). The smaller $Leu^{H47}$ allows bulky $Trp^{H50}$, which is normally in contact with $Trp^{H47}$, to rotate its indole ring about 120° along the $C^{\alpha}$-$C^{\beta}$ bond ($\chi_1$) toward $Leu^{H47}$ and fill in the vacated space near the bottom of the pocket. While maintaining similar hydrophobicity, this $Trp^{H50}$ side-chain rotation significantly deepens the active site so that the rigid and bulky hexachloronorbornene moiety of hapten **6** can be better accommodated.

The complementarity-determining region (CDR) H3 loops of all three antibodies are 10 amino acids long but highly variable in sequence, which reflects their origin from different combinations of D and J germ line gene segments and different VDJ junctions (*19*). Although residues H97, H100, and H100b contribute subtly to the shape of the pocket (Figs. 3 and 4), the shared length and canonical bulged torso conformation (*20*) of H3 appear to be more significant than a specific sequence for creating a generic binding site for hydrophobic haptens.

The crystal structure of 1E9 has provided an important impetus for biochemical characterization of its catalytic mechanism. The low solubility of the diene TCTD previously precluded a complete kinetic analysis of the antibody (*5*). By exploiting the observation that the bridgehead chlorine from the diene on the less deeply buried edge of hapten **6** is relatively solvent accessible (Fig. 3A), we have designed water-soluble dienes, such as thiophene dioxide **7** (*21*), that are good substrates for the antibody. Random, rapid equi-

**Table 1.** Data collection and refinement statistics. The Fab fragment of 1E9 was prepared by proteolytic digestion of intact IgG and purified by affinity chromatography on protein A and protein G columns as described (*12*). The hapten and 1E9 Fab fragment (about 22 mg/ml) were mixed in a 10:1 molar ratio for crystallization. Crystals were obtained from 14% PEG10K, 100 mM imidazolium malate (pH 5.5). Data were collected at −176°C with a crystal previously flash cooled in mother liquor containing 25% glycerol at Stanford Synchtrotron Radiation Laboratory (SSRL) beamline 9-1 with a MAR (MAR-Research) 30-cm area detector and processed with DENZO and SCALEPACK (*30*). The 1E9 structure was determined by molecular replacement using AMORE (*31*) with the DB3/progesterone complex (*14*) (PDB access code 1dbb) as the search model, yielding a correlation coefficient of 58.7 and $R_{cryst}$ of 40.2%. The hapten was built from an omit $F_o - F_c$ map only after several cycles of rebuilding and refinement of the Fab. The complex structure was refined with the conventional residual target function followed by the maximum likelihood target function of XPLOR (*32*). Because the aliphatic side chain of the hapten is largely disordered, only the rigid hexachloronorbornene moiety of the hapten was refined. The hapten side chain was later modeled by taking into account residual unconnected electron density in the binding site, followed by energy minimization. The 1E9 coordinates have been deposited in the Protein Databank (PDB access code 1c1e) and are available immediately from wilson@scripps.edu.

| | |
|---|---|
| Data collection | |
| Space group | $C222_1$ |
| Unit cell | $a$ = 44.73 Å, $b$ = 132.44 Å, $c$ = 167.50 Å |
| Resolution | 1.9 Å |
| Total observations | 126,249 |
| Unique reflections | 39,213 |
| $R_{sym}$ (%)* | 7.0 (83.6)† |
| Completeness (%) | 98.5 (99.4)† |
| Redundancy | 3.2 |
| $I/\sigma_I$‡ | 14.3 (1.2)† |
| Refinement | |
| Total residues | 435 |
| Water molecules | 195 |
| Nonpeptide residues | 2 |
| Refinement range | 20.0–1.9 |
| $R_{cryst}$ (%)§ | 23.9 (29.9)† |
| $R_{free}$ (%)¶ | 29.4 (31.8)† |
| Bond length deviation (Å) | 0.012 |
| Bond angle deviation (°) | 1.70 |
| Average $B$ value of protein atoms (Å$^2$) | 31.1 |
| Average $B$ value of hapten (Å$^2$) | 39.5 |
| Average $B$ value of water (Å$^2$) | 44.5 |

*$R_{sym} = \Sigma|F_o^2 - F_c^2|/\Sigma F_o^2$. †Values for data in outer shell of 1.9 to 1.95 Å. ‡Signal-to-noise ratio. §$R_{work} = \Sigma|F_o - F_c|/\Sigma|F_o|$, where $F_o$ and $F_c$ are the observed and calculated structure factors, respectively. ¶$R_{free}$ is calculated in the same manner as $R_{cryst}$ but from 5% of the data that were not used for refinement.

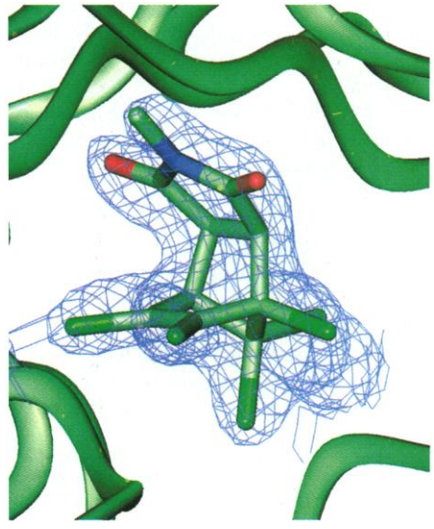

**Fig. 2.** Electron density for the hapten in the 1E9 binding pocket. The $F_o - F_c$ omit map contoured at 1.0σ level is shown as a close-up view looking down into the antibody combining site. The solvent-exposed linker of the hapten is not shown because of disorder. Figure prepared with QUANTA [Molecular Simulations Inc. (MSI)].

librium kinetics can now be observed (*22*) with a catalytic rate constant ($k_{cat}$) of 13 $min^{-1}$ and Michaelis constants ($K_m$) of 2.4 and 29 mM for **7** and NEM, respectively, at 15°C. The second-order rate constant for the background reaction, $k_{uncat}$, was found to be 0.013 $M^{-1}$ $min^{-1}$, giving an "effective molarity" (EM = $k_{cat}/k_{uncat}$) of 1000 M per binding site. Reactions with **1** are likely to be more efficient still, because it is processed three to four times more rapidly than **7** at similar diene concentrations. For comparison, DB3 gives no detectable catalysis of this reaction, whereas 39-A11 promotes its own cycloaddition (Fig. 1C) with an EM of only 0.35 M (*7*), and other reported antibody Diels-Alderases have EMs rarely exceeding 10 M (*8–10*).

The 1E9 structure reveals a binding pocket preorganized to maximize shape complementarity with the hapten through a myriad of van der Waals contacts, π-stacking with the flat, electron-deficient maleimide moiety, and a strategically placed hydrogen bond. Nevertheless, 1E9 does not appear to function as a classic entropy trap (*23*). The temperature dependence of $k_{cat}$ for the reaction between NEM and **7** gives values for the enthalpy and entropy of activation ($\Delta H^{\ddagger}$ and $\Delta S^{\ddagger}$) of 11.3 ± 0.2 kcal/mol and −22.1 ± 0.5 cal $K^{-1}$ $mol^{-1}$, respectively. The corresponding values for the uncatalyzed bimolecular cycloaddition are 15.5 ± 0.2 kcal/mol and −21.5 ± 0.6 cal $K^{-1}$ $mol^{-1}$. Thus, the rate of acceleration of 1E9 derives entirely from a lowering of the enthalpic barrier to catalysis. Because the reactants are collected together in the binding site, an entropy of reaction at least 10 cal $K^{-1}$ $mol^{-1}$ less negative than in solution might have been expected (*24*). The fact that the solution and antibody-catalyzed processes are equally unfavorable entropically could arise from restrictions of antibody motion upon binding of the transition state.

The relatively nonpolar milieu of protein pockets has been invoked as the source of acceleration for some antibody and enzyme-catalyzed reactions [(*25*), but see (*26*)]. However, a simple medium effect cannot account for the catalytic activity of 1E9 either, because the uncatalyzed reaction is 10 times slower in acetonitrile than in water (*22*). Free energies calculated by linear interaction energy (LIE) (*27*) show that binding of all species along the reaction coordinate is dominated by favorable van der Waals interactions. Nevertheless, such interactions provide rather poor discrimination between the reactant complex ($\alpha\Delta V_{vdw}$ = 12.7 kcal/mol) and transition state **5** ($\alpha\Delta V_{vdw}$ = 13.2 kcal/mol). In contrast, electrostatic interactions become less favorable upon reactant binding but are significantly improved in the transition state (*27*), largely because of the increased strength of the hydrogen bond from $Asn^{H35}$ to the carbonyl oxygen of the dienophile in the transition state. Enthalpic stabilization of the actual transition state by an unusually close fit with the largely hydrophobic binding pocket of the antibody, punctuated by one strategically placed polar functionality, thus explains the catalytic efficiency of 1E9. This mechanism is specified by the well-designed hapten, which closely resembles the rate-determining transition state (Fig. 1A).

The much lower catalytic efficiency of 39-A11 can be attributed, in large part, to the loose fit of its transition state to the binding site (*15*). Poor packing of the reaction center is exacerbated by incorporation of an ethano bridge in the hapten **9**, which has no counterpart in transition state **12** (Fig. 1, B and C). Consistent with this notion, the catalytic rate constant of 39-A11 was increased 5- to 10-fold by introducing site-directed mutations that improved packing interactions (*28*). Furthermore, in contrast to the 1E9-catalyzed reaction with its two electron-deficient addends, the cycloaddition catalyzed by 39-A11 involves a strong donor diene and acceptor dienophile. Hence, its transition state is much more polar than the ground state. Although this species will be stabilized by the same hydrogen bond between $Asn^{H35}$ and the dienophile carbonyl, the 39-A11 reaction will be disfavored by the relatively nonpolar environment of the binding site. These two competing factors may offset each other, consistent with the small net acceleration by 39-A11. Similar considerations may apply to 13G5, another Diels-Alderase antibody (EM = 6 M) (*9*), in which the role of hydrogen bonding on stereoselectivity has been established (*29*).

These results highlight the advantages of studying what might be regarded as non-optimized, early intermediates on the pathway to catalytic perfection instead of working backward from the highly evolved forms of natural enzymes. One can then discover the leaps in catalytic efficiency that arise from unanticipated mutations. Our combined structural, biochemical, and

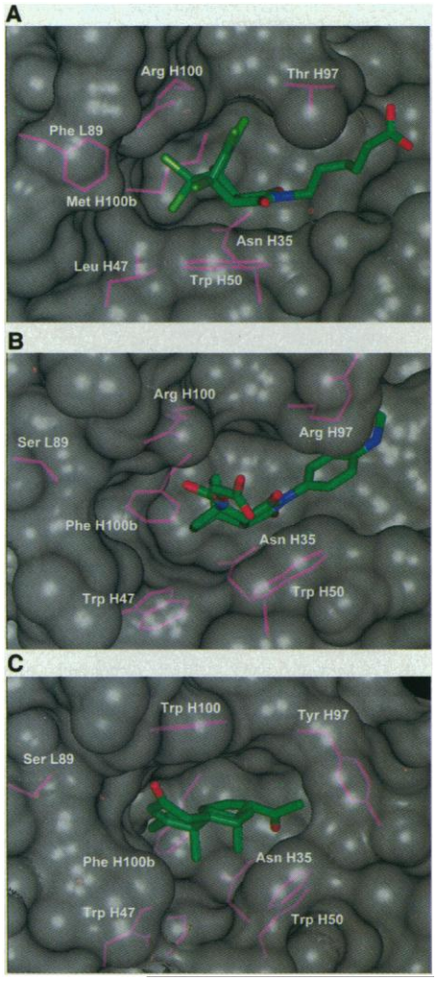


**Fig. 3.** Comparison of molecular surfaces of the related antibody combining sites. View is from the top of the binding site showing the fit of the cognate ligands of 1E9 (**A**), 39-A11 (*15*) (**B**), and DB3 (*14*) (**C**). In magenta, under the surface, the side chains of the ligand-contacting residues of each antibody are shown. Note the variation of the shape of the binding site of 1E9 due to the side-chain conformational change in $Trp^{H50}$ that results from the framework $Trp^{H47}$ → Leu substitution. Also, the $Asn^{H35}$ hydrogen bond with a ligand carbonyl oxygen is conserved in all three antibody combining sites. Figure prepared with Insight II (MSI).

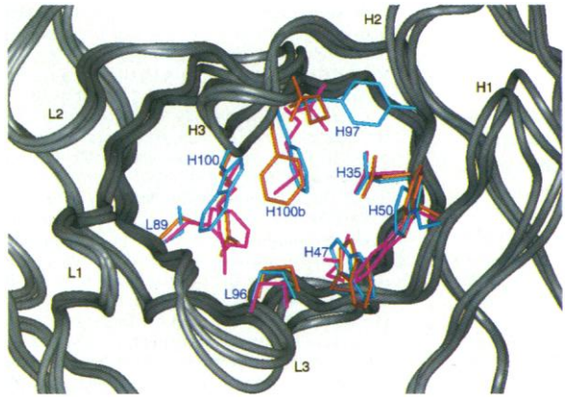


**Fig. 4.** Comparison of binding pockets for the three related antibodies. View into the antibody combining site showing the hapten contact residues (blue) for 1E9 (magenta), 39-A11 (gold), and DB3 (cyan). CDR loops are labeled (black) as L1 to L3 (light) and H1 to H3 (heavy chain).

**Table 2.** Comparison of related antibody-hapten complexes of three antibodies,1E9, DB3, and 39-A11 from the same germ line gene family. Buried surface areas were calculated by the program MS (*33*) with a probe of radius of 1.4 Å. The cavity volume between the ligand and the antibody was calculated by MS (*33*) with a probe of radius of 1.2 Å. Smaller gap index values indicate tighter packing and hence better shape complementarity between ligand and antibody (*34*).

| | 1E9·**6** | DB3·**8** | 39-A11·**9** |
|---|---|---|---|
| Buried surface of antibody upon binding (Å$^2$) | 343 | 285 | 279 |
| Buried surface of hapten upon binding (%) | 83.6 | 80.2 | 65.5 |
| Cavities* found between antibody and hapten (Å$^3$) | None | 19 | 117 |
| Contacts of hapten made to the antibody within van der Waals distance | 121 | 62 | 85 |
| Gap index (Å) | 0.44 | 0.90 | 1.69 |

*Cavity is defined as the enclosed space on the interface between hapten and antibody of the molecular contact surface traced by a probe of radius 1.2 Å with the MS program (*33*). Both volume and surface were calculated with GRASP (*34*).

quantum mechanical studies illustrate the steps that were necessary to attain exquisite shape complementarity of antibody and transition state and the consequent increase in efficiency of a chemical reaction of fundamental theoretical and practical interest. The opportunity to compare two highly related Diels-Alder antibodies that have arisen from the same germ line progenitor illustrates the interplay between binding energy and catalysis. What might be regarded as relatively innocuous mutations in the antibody combining site led to significant changes in its shape and, as a result, to almost perfect complementarity with the immunizing hapten. Judicious design of the transition state analog to enhance both chemical and shape mimicry of the actual Diels-Alder transition state has enabled the full extent of this shape complementarity to be converted into a more efficient catalytic outcome. It is evolution by such incremental steps that has permitted natural enzymes to attain their extraordinary catalytic efficiency. This study indicates that it is possible to evolve efficient catalysts, even unknown in nature, through remarkably subtle manipulations of an existing template.

### References and Notes


1. L. Pauling, *Am. Sci.* **36**, 51 (1948); W. P. Jencks, *Catalysis in Chemistry and Enzymology* (McGraw-Hill, New York, 1969).
2. P. G. Schultz and R. A. Lerner, *Science* **269**, 1835 (1995); *Acc. Chem. Res.* **26**, 391 (1993); D. Hilvert, *Top. Stereochem.* **22**, 83 (1999).
3. S. Laschat, *Angew. Chem. Int. Ed. Engl.* **35**, 289 (1996).
4. M. R. Haynes, E. A. Stura, D. Hilvert, I. A. Wilson, *Science* **263**, 646 (1994); P. A. Patten *et al., Science* **271**, 1086 (1996); G. J. Wedemayer, P. A. Patten, L. H. Wang, P. G. Schultz, R. C. Stevens, *Science* **276**, 1665 (1997); J. B. Charbonnier *et al., Science* **275**, 1140 (1997); H. D. Ulrich *et al., Nature* **389**, 271 (1997).
5. D. Hilvert, K. W. Hill, K. D. Nared, M.-T. M. Auditor, *J. Am. Chem. Soc.* **111**, 9261 (1989).
6. Quantum mechanical calculations at the RHF/6-31G(d) level were performed to optimize the geometries of reactants, intermediates, and transition states; energies were evaluated at the B3LYP/6-31G(d) level. Stationary points were characterized by RHF/3-21G frequency calculations (M. J. Frisch *et al., Gaussian*, Gaussian Inc., Pittsburgh, PA). The calculations show transition state **5** to be rate determining. The computed activation energy is 19.9 kcal/mol and increases to 22.1 kcal/mol in water (SCI-PCM) [M. Cossi *et al., Chem. Phys. Lett.* **255**, 327 (1996)]. A single hydrogen bond from a water molecule to NEM **2** lowers the activation energy by 0.6 kcal/mol. Calculations predict no effect on hydrogen bonding of water to the thiophene dioxide.
7. A. C. Braisted and P. G. Schultz, *J. Am. Chem. Soc.* **112**, 7430 (1990).
8. V. E. Gouverneur *et al., Science* **275**, 1140 (1997); A. A. P. Meekel, M. Resmini, U. K. Pandit, *J. Chem. Soc. Chem. Commun.* 571 (1995).
9. J. T. Yli-Kauhaluoma *et al., J. Am. Chem. Soc.* **117**, 7041 (1995).
10. A. R. Pitt, W. H. Stimson, C. J. Suckling, J. J. Marrero-Tellado, C. Vazzana, *Israel J. Chem.* **136**, 171 (1996).
11. B. Seelig and A. Jäschke, *Chem. Biol.* **6**, 167 (1999); T. M. Tarasow, S. L. Tarasow, B. E. Eaton, *Nature* **389**, 54 (1997).
12. E. A. Stura, G. G. Fieser, I. A. Wilson, *Immunomethods* **3**, 164 (1993). The full length IgG1 was expressed from mouse myeloma cells and purified as described in (*5*). The 1E9 Fab fragment was generated by enzymatic digestion with 2% papain in the presence of cysteine.
13. M. R. Haynes, M. Lenz, M. J. Taussig, I. A. Wilson, D. Hilvert, *Israel J. Chem.* **36**, 151 (1996).
14. J. H. Arevalo, M. J. Taussig, I. A. Wilson, *Nature* **365**, 859 (1993); J. H. Arevalo *et al., J. Mol. Biol.* **231,** 103 (1993); J. H. Arevalo *et al., J. Mol. Biol.* **241,** 663 (1994).
15. F. E. Romesberg, B. Spiller, P. G. Schultz, R. C. Stevens, *Science* **279**, 1929 (1998).
16. S. Jones and J. M. Thornton, *Proc. Natl. Acad. Sci. U.S.A.* **93**, 1320 (1996).
17. G. M. Morris *et al., J. Comp. Chem.* **19**, 1639 (1998); G. M. Morris *et al., J. Comput. Aided Mol. Des.* **10**, 293 (1996); D. S. Goodsell and A. J. Olson, *Proteins Struct. Funct. Genet.* **8**, 195 (1990).
18. E. A. Kabat, T. T. Wu, H. M. Perry, K. S. Gottesman, C. Foeller, *Sequences of Proteins of Immunological Interest* (U.S. Public Health Service, National Institutes of Health, Bethesda, MD, ed. 5, 1991). See also the antibody database Web page http://www.biochem.ucl.ac.uk/~martin/abs/
19. The DJ regions of the $V_H$ gene of 1E9 come from its germ line precursor, DFL 16.1 and $J_H4$, respectively, with very common guanine-rich joints flanking both ends of the D gene, whereas those of DB3 most likely come from SP25.8 and $J_H1$ with short VD and DJ junctions. For 39-A11, the DJ regions are most likely from DSP2.2 and $J_H2$ but with an uncommon nine-nucleotide VD junction. For 1E9, the use of the $J_H4$ minigene places a Met at position H100b, providing a hydrophobic floor for the binding pocket that is highly adaptable to the ligand shape because of the flexibility of its side chain; DB3 and 39-A11 utilize $J_H1$ and $J_H3$, respectively, resulting in a Phe at this position. Residue H100, which provides one of the walls of the cavity, arises from the DJ junction; it is an Arg in 1E9 and 39-A11 and a Trp in DB3. The H97 residue (Thr in 1E9, Tyr in DB3, and Arg in 39-A11) interacts primarily with the linker moiety in the 1E9 and 39-A11 structures, whereas in DB3 it provides a lid over one end of the hydrophobic cavity.
20. V. Morea, A. Tramontano, M. Rustici, C. Chothia, A. M. Lesk, *J. Mol. Biol.* **275**, 269 (1998).
21. Synthesis of **7**: 3,4,5-trichloro-2-thienylmethanol was reacted with ethyl iodoacetate under basic solid-liquid phase-transfer conditions to afford ethyl (3,4,5-trichlorothiophen-2-ylmethoxy) acetate in 69% yield based on recovered alcohol. The ester was quantitatively saponified and the resulting acid was oxidized with HOF-$CH_3CN$ to give **7** (73%). All new compounds gave satisfactory spectroscopic data.
22. Reactions were carried out in 50 mM acetate buffer (pH 5.5) containing 20 mM NaCl and were monitored either by high-pressure liquid chromatography or by starch-$I_2$ bleaching at 606 nm. Initial velocities were determined at several concentrations of one substrate while the concentration of the other was kept constant. The uncatalyzed reaction was carried out under identical conditions and also in acetonitrile.
23. F. H. Westheimer, *Adv. Enzymol.* **24**, 441 (1962).
24. M. I. Page and W. P. Jencks, *Proc. Natl. Acad. Sci. U.S.A.* **68**, 1678 (1971).
25. C. Lewis, T. Krämer, S. Robinson, D. Hilvert, *Science* **253**, 1019 (1991); S. N. Thorn, R. G. Daniels, M.-T. M. Auditor, D. Hilvert, *Nature* **373**, 228 (1995); F. Hollenfelder, A. J. Kirby, D. Tawfik, *Nature* **383**, 60 (1996); K. Kikuchi and D. Hilvert, *J. Am. Chem. Soc.* **118**, 8184 (1996).
26. A. Warshel and J. Florian, *Proc. Natl. Acad. Sci. U.S.A.* **95**, 5950 (1998).
27. Molecular dynamics simulations with the LIE method [J. Åqvist, C. Medina, J. E. Samuelsson, *Protein Eng.* **7**, 385 (1994)], derived from linear response theory, were used to compute and analyze binding of reactants and transition states to the antibody. The free energy of binding is calculated as $\Delta G_{bind} = 1/2\ \Delta V_{elec} + \alpha \Delta V_{vdw}$, where $\Delta V_{elec}$ and $\Delta V_{vdw}$ denote the difference of ensemble-averaged electrostatic and van der Waals interaction energies between the antibody-bound and aqueous-solvated states. The parameter $\alpha$ was obtained from fitting to known binding affinities of steroids to DB3 (*14*). Molecular dynamics simulations were computed with a modified version of AMBER4.1 (D. A. Pearlman *et al.*, AMBER4.1, University of California, San Francisco, 1995). The free energy of binding of **1** plus **2** into a complex in the antibody is computed as −3.2 kcal/mol, compared with experimental values of −5.2 kcal/mol from $K_m$ values. The free energy of binding of transition state **5** is −8.9 kcal/mol. Thus, the predicted activation energy of the cycloaddition is lowered 5.7 kcal/mol relative to that in water (*6*).
28. F. E. Romesberg and P. G. Schultz, *Bioorg. Med. Chem. Lett.* **9**, 1741 (1999).
29. A. Heine *et al., Science* **279**, 1934 (1998).
30. Z. Otwinowski and W. Minor, *Methods Enzymol.* **276**, 307 (1997).
31. J. Navaza, *Acta Crystallogr.* **A50**, 157 (1994).
32. A. T. Brünger, *X-PLOR, Version 3.1: A System for X-Ray and NMR* (Yale Univ. Press, New Haven, CT, 1992); J. Badger *et al., Proteins Struct. Funct. Genet.* **35**, 25 (1999).
33. M. L. Connolly, *J. Appl. Crystallogr.* **16**, 439 (1983).
34. The molecular surfaces of the antibody, antigen, and antibody-antigen complex were constructed separately with the program GRASP [A. Nicholls, K. A. Sharp, B. Honig, *Proteins Struct. Funct. Genet.* **11**, 281 (1991)] with a probe radius of 1.4 Å, and the volume enclosed in each surface was then computed. The gap volume is taken as the difference between the volume of the complex and the sum of the volumes of the antibody and the antigen. Gap index is the gap volume divided by the buried surface area.


35. Supported by NIH grants CA27489 (I.A.W.) and GM38273 (D.H.) and NSF grant CHE-9616772 (K.N.H.). We thank T. Horton, N. Jiang, and M. Auditor for technical assistance; the staff of SSRL beamline 9-1; R. A. Lerner, A. Heine, and D. J. Edwards for helpful discussions; the referees for helpful comments; N. R. Klinman for advice on germ line gene analysis; and K. Renner for computational assistance.

30 July 1999; accepted 2 November 1999

## References and Notes

[2] **From Molecular Diversity to Catalysis: Lessons from the Immune System**

Peter G. Schultz; Richard A. Lerner

*Science*, New Series, Vol. 269, No. 5232. (Sep. 29, 1995), pp. 1835-1842.

Stable URL:

http://links.jstor.org/sici?sici=0036-8075%2819950929%293%3A269%3A5232%3C1835%3AFMDTCL%3E2.0.CO%3B2-U

[4] **Routes to Catalysis: Structure of a Catalytic Antibody and Comparison with Its Natural Counterpart**

Matthew R. Haynes; Enrico A. Stura; Donald Hilvert; Ian A. Wilson

*Science*, New Series, Vol. 263, No. 5147. (Feb. 4, 1994), pp. 646-652.

Stable URL:

http://links.jstor.org/sici?sici=0036-8075%2819940204%293%3A263%3A5147%3C646%3ARTCSOA%3E2.0.CO%3B2-I

[4] **The Immunological Evolution of Catalysis**

Phillip A. Patten; Nathanael S. Gray; Priscilla L. Yang; Cara B. Marks; Gary J. Wedemayer; J. Jay Boniface; Raymond C. Stevens; Peter G. Schultz

*Science*, New Series, Vol. 271, No. 5252. (Feb. 23, 1996), pp. 1086-1091.

Stable URL:

http://links.jstor.org/sici?sici=0036-8075%2819960223%293%3A271%3A5252%3C1086%3ATIEOC%3E2.0.CO%3B2-Y

# LINKED CITATIONS



[4] **Structural Insights into the Evolution of an Antibody Combining Site**

Gary J. Wedemayer; Phillip A. Patten; Leo H. Wang; Peter G. Schultz; Raymond C. Stevens

*Science*, New Series, Vol. 276, No. 5319. (Jun. 13, 1997), pp. 1665-1669.

Stable URL:

http://links.jstor.org/sici?sici=0036-8075%2819970613%293%3A276%3A5319%3C1665%3ASIITEO%3E2.0.CO%3B2-V

[4] **Structural Convergence in the Active Sites of a Family of Catalytic Antibodies**

Jean-Baptiste Charbonnier; Béatrice Golinelli-Pimpaneau; Benoît Gigant; Dan S. Tawfik; Rachel Chap; Daniel G. Schindler; Se-Ho Kim; Bernard S. Green; Zelig Eshhar; Marcel Knossow

*Science*, New Series, Vol. 275, No. 5303. (Feb. 21, 1997), pp. 1140-1142.

Stable URL:

http://links.jstor.org/sici?sici=0036-8075%2819970221%293%3A275%3A5303%3C1140%3ASCITAS%3E2.0.CO%3B2-6

[15] **Immunological Origins of Binding and Catalysis in a Diels-Alderase Antibody**

Floyd E. Romesberg; Ben Spiller; Peter G. Schultz; Raymond C. Stevens

*Science*, New Series, Vol. 279, No. 5358. (Mar. 20, 1998), pp. 1929-1933.

Stable URL:

http://links.jstor.org/sici?sici=0036-8075%2819980320%293%3A279%3A5358%3C1929%3AIOOBAC%3E2.0.CO%3B2-3

[24] **Entropic Contributions to Rate Accelerations in Enzymic and Intramolecular Reactions and the Chelate Effect**

Michael I. Page; William P. Jencks

*Proceedings of the National Academy of Sciences of the United States of America*, Vol. 68, No. 8. (Aug., 1971), pp. 1678-1683.

Stable URL:

http://links.jstor.org/sici?sici=0027-8424%28197108%2968%3A8%3C1678%3AECTRAI%3E2.0.CO%3B2-T

[25] **Medium Effects in Antibody-Catalyzed Reactions**

Cristina Lewis; Thomas Krämer; Suzanne Robinson; Donald Hilvert

*Science*, New Series, Vol. 253, No. 5023. (Aug. 30, 1991), pp. 1019-1022.

Stable URL:

http://links.jstor.org/sici?sici=0036-8075%2819910830%293%3A253%3A5023%3C1019%3AMEIAR%3E2.0.CO%3B2-P

# LINKED CITATIONS



[26] **Computer Simulations of Enzyme Catalysis: Finding out what has been Optimized by Evolution**

Arieh Warshel; Jan Florian

*Proceedings of the National Academy of Sciences of the United States of America*, Vol. 95, No. 11. (May 26, 1998), pp. 5950-5955.

Stable URL:

http://links.jstor.org/sici?sici=0027-8424%2819980526%2995%3A11%3C5950%3ACSOECF%3E2.0.CO%3B2-K

[29] **An Antibody exo Diels-Alderase Inhibitor Complex at 1.95 Angstrom Resolution**

Andreas Heine; Enrico A. Stura; Jari T. Yli-Kauhaluoma; Changshou Gao; Qiaolin Deng; Brett R. Beno; Kendall N. Houk; Kim D. Janda; Ian A. Wilson

*Science*, New Series, Vol. 279, No. 5358. (Mar. 20, 1998), pp. 1934-1940.

Stable URL:

http://links.jstor.org/sici?sici=0036-8075%2819980320%293%3A279%3A5358%3C1934%3AAAEDIC%3E2.0.CO%3B2-E